IEEE Access
Multidisciplinary | Rapid Review | Open Access Journal

Received August 25, 2019, accepted September 6, 2019, date of publication September 18, 2019, date of current version October 1, 2019.

Digital Object Identifier 10.1109/ACCESS.2019.2942054

Nonlinear Output Feedback Control of Flexible Rope Crane Systems With State Constraints

NING SUN[1,2], (Senior Member, IEEE), JIANYI ZHANG[1], XIN XIN[2], (Senior Member, IEEE), TONG YANG[1], AND YONGCHUN FANG[1], (Senior Member, IEEE)

[1]Institute of Robotics and Automatic Information Systems, College of Artificial Intelligence, Nankai University, Tianjin 300350, China
[2]Faculty of Computer Science and Systems Engineering, Okayama Prefectural University, Soja 719-1197, Japan

Corresponding author: Xin Xin (xxin@cse.oka-pu.ac.jp)

This work was supported in part by the National Key R&D Program of China under Grant 2018YFB1309000, in part by the National Natural Science Foundation of China under Grant 61873134 and Grant U1706228, in part by the Program of JSPS (Japan Society for the Promotion of Science) International Research Fellow under Grant 18F18363, and in part by the JSPS KAKENHI under Grant 17K06504.

ABSTRACT When the suspension rope of the crane system is relatively long and its mass cannot be simply ignored compared with that of the payload, or when the crane rope is underwater, it will exhibit flexible characteristics, that is, the bending deformation will occur during swing. Undoubtedly, unreasonable bending deformation of the crane rope will further excite larger-amplitude payload swing, which will seriously influence the efficiency and safety. To this end, for flexible rope crane systems, this paper carries out in-depth analysis and puts forward an effective control method. Specifically, by introducing the concept of lumped mass method and virtual spring, a nonlinear dynamic model is established. Furthermore, in order to solve the problem that velocity signals are not measurable, a nonlinear control strategy, which does not need velocity signals for feedback, is proposed in this paper. Finally, rigorous theoretical analysis and a series of experimental results verify the effectiveness of the proposed control strategy.

INDEX TERMS Cranes, swing elimination, positioning control, motion control.

I. INTRODUCTION

In recent decades, the control problem of underactuated and mechatronic systems have been a hot topic [1]–[15], among which crane systems are a typical representative. Due to the excellent capacity of cargo transportation, they have been widely used in construction sites, production workshops, ship terminals, and so on. Undoubtedly, the working status of crane systems greatly affects the production efficiency of related industries. With the improvement of industrialization, higher requirements are being put forward for the accuracy and efficiency of crane systems. However, at present, the automation level of crane systems is still unsatisfactory to some extent, since most crane systems still rely heavily on manual operation. There are many pratical problems associated with manual operation, such as low efficiency, poor safety, and so forth. Therefore, designing effective control methods for cranes is important from a practical perspective.

During the past few years, a lot of meaningful works have been made about crane control. The input shaping technique [16]–[19] is one of the most popularly used open-loop control methods at present. In addition, trajectory planning [20]–[22] is another effective open-loop control method. Furthermore, in order to increase robustness to counteract plant uncertainties and external disturbances, a series of closed-loop control algorithms are proposed. Those methods mainly include prediction control [23], flatness control [24], energy-based control [25]–[29], adaptive control [30]–[34], sliding-mode control [35]–[38], observer-based control [39], saturated control [40], optimal control [41], delayed reference control [42], intelligent control [43]–[51], and so on.

The aforementioned works are mostly based on rigid rope crane systems, which regard the crane rope as being rigid and assume that it does not bend during payload swing. Actually, in some special situations, the flexible characteristics of the crane rope cannot be simply roughly ignored [52]–[56]. For example, when the crane rope is long and its mass cannot be neglected compared with that of payload's (carrying out high altitude hoisting task), or when the crane rope is underwater (executing underwater lifting operation), due to the influence of winds or currents, the crane rope's flexible deformation may become apparent. The rope flexible deformation can

The associate editor coordinating the review of this manuscript and approving it for publication was Nishant Unnikrishnan.

further stimulate the large-scale payload swing, which will not only reduce the system lifting efficiency, but also easily lead to serious safety accidents. Therefore, it is essential to study the control problem of flexible rope crane systems.

There have been much fewer reported works on the control of flexible rope crane systems [52]–[56] than traditional rigid rope ones. In [52], Shah and Hong propose a novel boundary scheme for position and vibration control of a nuclear refueling machine (i.e., a special kind of flexible rope crane). An integral-barrier Lyapunov function is constructed to design a boundary control law to realize the control objective of flexible rope's bending restriction in [53]. In addition, reference [55] simplifies the model of flexible rope bridge cranes and further proposes a linear feedback controller with the crane rope deformation velocity signal. Furthermore, based on [55], a linear boundary feedback control law is designed in [56] on the basis of the reverse recursive method.

After a careful literature review, for flexible rope cranes, since much fewer works are reported, many open practical problems need to be solved. To do so, in this paper, we will propose a nonlinear output feedback control method for flexible rope cranes *without* utilizing velocity signal feedback or other signals which are difficult to measure. For practical cranes, the trolley motion range is limited, and the proposed method can theoretically ensure that the trolley never moves out of this range, which improves the control system safety. We provide Lyapunov-based mathematical analysis for the asymptotic stability. It is noted that, for most existing works on flexible cranes, *only simulation* results are provided. In contrast, in this study, we build a flexible cable crane experimental hardware platform, on which a series of hardware experiments have been carried out to verify the proposed controller's performance in different situations.

The structure of the paper is as follows. The dynamic model of flexible cable cranes is provided in Section II. Then, both controller design and stability analysis are provided in Section III. In Section IV, experimental results will verify the performance of the designed controller. In the end, some summaries are given in Section V.

II. CRANE DYNAMICS

The schematic diagram of flexible rope crane systems is shown in the left figure of Fig. 1. Unlike rigid rope cranes, the rope's flexible characteristics will be fully considered in flexible rope crane systems. In Fig. 1, M and m_2 represent the mass of the trolley and the payload, respectively, l denotes the length of the flexible crane rope, x is the trolley displacement, $z(y,t)$ stands for the transverse deflection of each point on the crane rope, which reflects the flexible characteristics, ϕ is the defined payload swing angle, which is expressed by the angle between the tangent line of payload position on flexible rope and the vertical direction, and f_x denotes the horizontal driving force applied to the trolley.

Since the characteristics of flexible rope crane systems are infinite-dimensional (involving partial differential equations (PDEs)) and very complex, the concept of the lumped mass

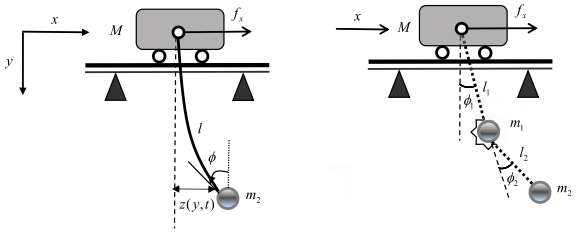

FIGURE 1. Flexible rope crane system (left: the original system model; right: the equivalent model).

method and virtual spring will be introduced to describe the flexible characteristics of the crane rope more intuitively. As shown in the right figure of Fig. 1, the curved crane rope is equivalent to two rigid ropes, and they are connected by a virtual spring with stiffness coefficient k. In the figure, m_1 denotes the equivalent mass of the crane rope, i.e., the distributed mass is equivalent to a lumped mass block, l_1 and l_2 are equivalent length of two rigid ropes, respectively, ϕ_1 represents the first pendulum angle, and ϕ_2 is the second deflection angle, which can be used to reflect the bending degree of the crane rope to a certain extent.

The total kinetic energy (containing the trolley, payload, and rope (equivalent mass block)), is depicted as follows:

$$\begin{aligned} K = {} & \frac{1}{2}M\dot{x}^2 + \frac{1}{2}m_1(\dot{x}^2 + 2\dot{x}\dot{\phi}_1 l_1\cos\phi_1 + l_1^2\dot{\phi}_1^2) \\ & + \frac{1}{2}m_2\Big[l_2^2(\dot{\phi}_1+\dot{\phi}_2)^2 + 2\dot{x}(\dot{\phi}_1+\dot{\phi}_2)l_2\cos(\phi_1+\phi_2) \\ & \quad + (\dot{x}^2 + 2\dot{x}\dot{\phi}_1 l_1\cos\phi_1 + l_1^2\dot{\phi}_1^2) \\ & \quad + 2l_1l_2\cos\phi_2\dot{\phi}_1^2 + 2l_1l_2\cos\phi_2\dot{\phi}_1\dot{\phi}_2\Big]. \end{aligned} \tag{1}$$

The total system potential energy includes the gravitational potential energy of the trolley, the crane rope, and the payload, and the elastic potential energy of the virtual spring. In this paper, the horizontal plane of the static payload is chosen as the zero potential energy surface. The following expression of the total system potential energy can be obtained:

$$\begin{aligned} P = {} & Mg(l_1+l_2) + m_1g(l_1+l_2-l_1\cos\phi_1) \\ & + m_2g[l_1+l_2-l_1\cos\phi_1 - l_2\cos(\phi_1+\phi_2)] \\ & + \frac{1}{2}k\phi_2^2, \end{aligned} \tag{2}$$

where g denotes the gravitational acceleration.

Then, Lagrange's method is used to establish the dynamic model of the flexible rope crane systems. Let (1) and (2) be inserted into the Lagrange equation indicated as follows:

$$\frac{d}{dt}\left(\frac{\partial L}{\partial \dot{\boldsymbol{q}}}\right) - \frac{\partial L}{\partial \boldsymbol{q}} = F, \tag{3}$$

where $L = K - P$ denotes the Lagrangian, F stands for the generalized force, and $\boldsymbol{q} = [x \;\; \phi_1 \;\; \phi_2]^\top$ is the system state vector. After a series of calculations, the system dynamic model can be obtained as follows:

$$\begin{aligned} & (M+m_1+m_2)\ddot{x} + [(m_1+m_2)l_1\cos\phi_1 \\ & \quad + m_2l_2\cos(\phi_1+\phi_2)]\ddot{\phi}_1 + m_2l_2\cos(\phi_1+\phi_2)\ddot{\phi}_2 \\ & \quad - [(m_1+m_2)l_1\sin\phi_1 + m_2l_2\sin(\phi_1+\phi_2)]\dot{\phi}_1^2 \\ & \quad - m_2l_2\sin(\phi_1+\phi_2)\dot{\phi}_2^2 - 2m_2l_2\sin(\phi_1+\phi_2)\dot{\phi}_1\dot{\phi}_2 \\ & \quad = f_x, \end{aligned} \tag{4}$$

$$
\begin{aligned}
&[(m_1+m_2)l_1\cos\phi_1+m_2l_2\cos(\phi_1+\phi_2)]\ddot{x}\\
&\quad+[(m_1+m_2)l_1^2+m_2l_2^2+2m_2l_1l_2\cos\phi_2]\ddot{\phi}_1\\
&\quad+(m_2l_2^2+m_2l_1l_2\cos\phi_2)\ddot{\phi}_2-m_2l_1l_2\sin\phi_2\dot{\phi}_2^2\\
&\quad-2m_2l_1l_2\sin\phi_2\dot{\phi}_1\dot{\phi}_2+(m_1+m_2)gl_1\sin\phi_1\\
&\quad+m_2gl_2\sin(\phi_1+\phi_2)=0, \qquad (5)\\
&m_2l_2\cos(\phi_1+\phi_2)\ddot{x}+(m_2l_1l_2\cos\phi_2+m_2l_2^2)\ddot{\phi}_1\\
&\quad+m_2l_2^2\ddot{\phi}_2+m_2l_1l_2\sin\phi_2\dot{\phi}_1^2\\
&\quad+m_2gl_2\sin(\phi_1+\phi_2)+k\phi_2=0. \qquad (6)
\end{aligned}
$$

Furthermore, the system model (4)-(6) can be rewritten into the following compact matrix-vector form:

$$M(\boldsymbol{q})\ddot{q}+V_n(\boldsymbol{q},\dot{\boldsymbol{q}})\dot{q}+G(\boldsymbol{q})=\boldsymbol{U}, \qquad (7)$$

where

$$
\begin{aligned}
M(\boldsymbol{q})&=\begin{bmatrix} m_{11} & m_{12} & m_{13}\\ m_{21} & m_{22} & m_{23}\\ m_{31} & m_{32} & m_{33}\end{bmatrix},\\
V_n(\boldsymbol{q},\dot{\boldsymbol{q}})&=\begin{bmatrix} v_{11} & v_{12} & v_{13}\\ v_{21} & v_{22} & v_{23}\\ v_{31} & v_{32} & v_{33}\end{bmatrix},\\
G(\boldsymbol{q})&=[0 \quad g_2 \quad g_3]^\top,\\
U(\boldsymbol{q},\dot{\boldsymbol{q}})&=[f_x \quad 0 \quad 0]^\top,
\end{aligned}
$$

where the expressions of each items are detailed as follows:

$$
\begin{aligned}
m_{11}&=M+m_1+m_2,\\
m_{12}&=(m_1+m_2)l_1\cos\phi_1+m_2l_2\cos(\phi_1+\phi_2),\\
m_{13}&=m_2l_2\cos(\phi_1+\phi_2),\\
m_{21}&=(m_1+m_2)l_1\cos\phi_1+m_2l_2\cos(\phi_1+\phi_2),\\
m_{22}&=(m_1+m_2)l_1^2+m_2l_2^2+2m_2l_1l_2\cos\phi_2,\\
m_{23}&=m_2l_2^2+m_2l_1l_2\cos\phi_2,\\
m_{31}&=m_2l_2\cos(\phi_1+\phi_2),\quad m_{32}=m_2l_2^2+m_2l_1l_2\cos\phi_2,\\
m_{33}&=m_2l_2^2,\\
v_{11}&=0,\\
v_{12}&=-(m_1+m_2)l_1\sin\phi_1\dot{\phi}_1\\
&\qquad-m_2l_2\sin(\phi_1+\phi_2)(\dot{\phi}_1+\dot{\phi}_2),\\
v_{13}&=-m_2l_2\sin(\phi_1+\phi_2)(\dot{\phi}_1+\dot{\phi}_2),\ v_{21}=0,\\
v_{22}&=-m_2l_1l_2\sin\phi_2\dot{\phi}_2,\quad v_{23}=-m_2l_1l_2\sin\phi_2(\dot{\phi}_1+\dot{\phi}_2),\\
v_{31}&=0,\ v_{32}=m_2l_1l_2\sin\phi_2\dot{\phi}_1,\\
v_{33}&=0,\\
g_2&=(m_1+m_2)gl_1\sin\phi_1+m_2gl_2\sin(\phi_1+\phi_2),\\
g_3&=m_2gl_2\sin(\phi_1+\phi_2)+k\phi_2.
\end{aligned}
$$

Regarding flexible rope crane systems, the control objectives are to not only achieve accurate trolley positioning and payload anti-swing control, but also restrict the rope's flexible bending. In (4)-(6), the payload swing angle $\phi(t)$ is determined by the first swing angle $\phi_1(t)$ and the second deflection angle $\phi_2(t)$, that is, if $\phi_1(t)$ and $\phi_2(t)$ are 0, then the payload swing angle $\phi(t)$ will also be identical to 0. Moreover, the bending degree of the crane rope is related to the second deflection angle $\phi_2(t)$; thus the aim of restricting payload swing and rope bending can be converted into that of restricting of the first swing angle $\phi_1(t)$ and the second order deflection angle $\phi_2(t)$.

Based on the expressions of matrices $M(\boldsymbol{q})$ and $V_n(\boldsymbol{q},\dot{\boldsymbol{q}})$, the following two important properties can be shown to hold:

Property 1: $M(\boldsymbol{q})$ is a positive definite symmetric matrix.

Property 2: $1/2\dot{M}(\boldsymbol{q})-V_n(\boldsymbol{q},\dot{\boldsymbol{q}})$ is skew-symmetric.

Meanwhile, as widely done in the literature, the following assumption is made [16]–[56]:

Assumption 1: The swing angles are within the following range:

$$-\tfrac{\pi}{2}<\phi_i<\tfrac{\pi}{2},\ i=1,2. \qquad (8)$$

III. OUTPUT FEEDBACK CONTROLLER DESIGN

We will propose in this section a nonlinear output feedback controller for flexible rope crane systems, which is independent of model parameters, does not need velocity signals, and can guarantee the trolley motion range.

A. VIRTUAL SPRING-MASS SYSTEM-BASED VELOCITY ESTIMATOR

The system mechanical energy can be expressed as follows:

$$E_m=\tfrac{1}{2}\dot{\boldsymbol{q}}^\top M(\boldsymbol{q})\dot{\boldsymbol{q}}+P. \qquad (9)$$

The first term in (9) represents the total system kinetic energy, and the second term denotes the potential energy of the system. Combining the derivative of (9) with the Property 1 and Property 2, we can obtain that

$$
\begin{aligned}
\dot{E}_m&=\dot{\boldsymbol{q}}^\top M(\boldsymbol{q})\ddot{\boldsymbol{q}}+\frac{1}{2}\dot{\boldsymbol{q}}^\top\dot{M}(\boldsymbol{q})\dot{\boldsymbol{q}}+m_1gl_1\sin\phi_1\dot{\phi}_1\\
&\quad+m_2gl_1\sin\phi_1\dot{\phi}_1+m_2gl_2\sin(\phi_1+\phi_2)\\
&\quad\times(\dot{\phi}_1+\dot{\phi}_2)+k\phi_2\\
&=\dot{\boldsymbol{q}}^\top[U(\boldsymbol{q},\dot{\boldsymbol{q}})-V_n(\boldsymbol{q},\dot{\boldsymbol{q}})\dot{\boldsymbol{q}}-G(\boldsymbol{q})]\\
&\quad+\frac{1}{2}\dot{\boldsymbol{q}}^\top\dot{M}(\boldsymbol{q})\dot{\boldsymbol{q}}+m_1gl_1\sin\phi_1\dot{\phi}_1\\
&\quad+m_2gl_1\sin\phi_1\dot{\phi}_1+m_2gl_2\sin(\phi_1+\phi_2)\\
&\quad\times(\dot{\phi}_1+\dot{\phi}_2)+k\phi_2\\
&=\dot{\boldsymbol{q}}^\top U(\boldsymbol{q},\dot{\boldsymbol{q}})+\dot{\boldsymbol{q}}^\top\left(\frac{1}{2}\dot{M}(\boldsymbol{q})-V_n(\boldsymbol{q},\dot{\boldsymbol{q}})\right)\dot{\boldsymbol{q}}\\
&=\dot{\boldsymbol{q}}^\top U(\boldsymbol{q},\dot{\boldsymbol{q}})=\dot{x}f_x. \qquad (10)
\end{aligned}
$$

Obviously, from (10), it can be seen that the flexible rope crane system, which takes the trolley horizontal velocity $\dot{x}(t)$ as the output, the driving force f_x as the input, and the mechanical energy $E_m(t)$ as the energy storage function, is a typical passive system.

In many practical applications, velocity signals may be difficult to be directly measured. Therefore, in order to avoid using velocity signals as feedback, a *virtual spring-mass system* is introduced to replace velocity signals. The subsequent stability analysis will verify the effectiveness of the designed estimator. The virtual spring-mass system is designed as

follows:

$$m_v\ddot{x}_v = -k_v(x_v - x) - c\dot{x}_v, \tag{11}$$

where m_v is the mass of the virtual mass, x_v corresponds to its displacement, k_v and c represent the stiffness coefficient and the virtual damping coefficient, respectively. It will become apparent in the subsequent stability analysis that, by involving (11) in the to-be-designed controller, velocity signals are not needed as feedback.

B. CONTROLLER DESIGN

Firstly, the following trolley positioning error is defined:

$$e(t) = x(t) - x_d, \tag{12}$$

where x_d represents the target position of the trolley.

At the same time, in order to further improve the operation safety, the following motion range constraint for the trolley needs to be met:

$$x_m < x(t) < x_M, \ \forall t \geq 0, \tag{13}$$

where $x_M \geq x_d$ and $0 < x_m < x_d$ denote the upper and lower bounds of the trolley motion range, respectively.

Based on the system mechanical energy given in (9), we can construct the following Lyapunov function candidate:

$$\begin{aligned} V(t) = E_m + \frac{k_p}{2}e^2 + \frac{1}{2}[m_v\dot{x}_v^2 + k_v(x_v - x)^2] \\ + \frac{k_\chi e^2}{2}\left[\frac{1}{(x - x_M)^2} + \frac{1}{(x - x_m)^2}\right], \end{aligned} \tag{14}$$

wherein k_p and k_χ are positive constants.

By calculating the derivative of (14) with respect to time t, and further combining equation (10) and (11), it can be obtained that

$$\begin{aligned} \dot{V}(t) &= \dot{E}_m + k_p e\dot{e} + m_v\ddot{x}_v\dot{x}_v + k_v(x_v - x)(\dot{x}_v - \dot{x}) \\ &\quad + k_\chi e\dot{e}\left[\frac{x_d - x_M}{(x - x_M)^3} + \frac{x_d - x_m}{(x - x_m)^3}\right] \\ &= \dot{x}f_x + k_p e\dot{e} + [-k_v(x_v - x) - c\dot{x}_v]\dot{x}_v \\ &\quad + k_v(x_v - x)(\dot{x}_v - \dot{x}) \\ &\quad + k_\chi e\dot{e}\left[\frac{x_d - x_M}{(x - x_M)^3} + \frac{x_d - x_m}{(x - x_m)^3}\right] \\ &= \dot{x}\left(f_x + k_p e - k_v(x_v - x)\right. \\ &\quad \left. + k_\chi e\left[\frac{x_d - x_M}{(x - x_M)^3} + \frac{x_d - x_m}{(x - x_m)^3}\right]\right) - c\dot{x}_v^2. \end{aligned} \tag{15}$$

According to the obtained form of (15), the following controller is designed:

$$\begin{aligned} f_x = &-k_p e + k_v(x_v - x) \\ &- k_\chi e\left[\frac{x_d - x_M}{(x - x_M)^3} + \frac{x_d - x_m}{(x - x_m)^3}\right]. \end{aligned} \tag{16}$$

C. STABILITY ANALYSIS

In this subsection, the closed-loop system asymptotic stability will be analyzed.

Theorem 1: The designed controller (16) can achieve precise trolley positioning and simultaneously effectively restrict the payload swing of flexible cranes, in the sense that,

$$\begin{aligned} \lim_{t\to\infty}&\begin{bmatrix} x & \phi_1 & \phi_2 & \dot{x} & \dot{\phi}_1 & \dot{\phi}_2 \end{bmatrix}^\top \\ &= \begin{bmatrix} x_d & 0 & 0 & 0 & 0 & 0 \end{bmatrix}^\top. \end{aligned}$$

Proof: By substituting the designed controller (16) into (15), one can obtain that

$$\dot{V}(t) = -c\dot{x}_v^2 \leq 0, \tag{17}$$

which shows that $\dot{V}(t)$ is negative semi-definite, and hence,

$$0 < V(t) \leq V(0) \ll +\infty. \tag{18}$$

Further, we first analyze that the constraint of (13) is assured. To apply reduction to absurdity, we assume that the trolley displacement $x(t)$ is going to exceed the given bound, i.e., $x(t) > x_M$ or $x(t) < x_m$; then, due to the continuity of closed-loop system trajectories, there must be a time instant t_J such that $x(t_J) = x_m$ or $x(t_J) = x_M$ holds. Furthermore, according to the expression of (14), one can see that $V(t)$ will tend to be positive *infinite* at t_J, which contradicts the conclusion in (18). Therefore, the trolley displacement does not exceed the range during the entire process, i.e.,

$$x_m < x(t) < x_M, \ \forall t \geq 0. \tag{19}$$

Then, according to (18), one sees that $V(t)$ is bounded, and based on the structure of $V(t)$, it is easy to know

$$\begin{aligned} E_m,\ e,\ x_v - x \in L_\infty &\Rightarrow x,\ x_v,\ \dot{x},\ \dot{\phi}_1,\ \dot{\phi}_2 \in L_\infty \\ &\Rightarrow f_x \in L_\infty. \end{aligned} \tag{20}$$

Next, we define S as the largest invariant set that is contained in following set:

$$S = \left\{(x,\ \phi_1,\ \phi_2,\ \dot{x},\ \dot{\phi}_1,\ \dot{\phi}_2) \mid \dot{V}(t) = 0\right\}.$$

According to the form of $\dot{V}(t)$ in (17), one can derive that, within the invariant set of S,

$$\dot{x}_v = 0, \tag{21}$$

which infers that $\ddot{x}_v = 0$ in S. Furthermore, along with (11), it can be inferred that within S,

$$x_v - x = 0 \Rightarrow x_v = x. \tag{22}$$

Due to $\dot{x}_v = 0$, x_v is a constant within S; along with (22), it is known that x is also a constant. Therefore,

$$\dot{x} = 0. \tag{23}$$

Then, it is further indicated that

$$\ddot{x} = 0,\ e = c_1,\ x = \lambda, \tag{24}$$

where both c_1 and λ are constants.

By substituting (22), (23), and (24) into (4)-(6), one can obtain that

$$\begin{aligned}&[(m_1+m_2)l_1\cos\phi_1+m_2l_2\cos(\phi_1+\phi_2)]\ddot{\phi}_1\\&\quad+m_2l_2\cos(\phi_1+\phi_2)\ddot{\phi}_2-[(m_1+m_2)l_1\sin\phi_1\\&\quad+m_2l_2\sin(\phi_1+\phi_2)]\dot{\phi}_1^2-m_2l_2\sin(\phi_1+\phi_2)\dot{\phi}_2^2\\&\quad-2m_2l_2\sin(\phi_1+\phi_2)\dot{\phi}_1\dot{\phi}_2\\&\qquad=-c_1\left(k_p+k_\chi\left[\frac{x_d-x_M}{(\lambda-x_M)^3}+\frac{x_d-x_m}{(\lambda-x_m)^3}\right]\right),\end{aligned}\tag{25}$$

$$\begin{aligned}&[(m_1+m_2)l_1^2+m_2l_2^2+2m_2l_1l_2\cos\phi_2]\ddot{\phi}_1\\&\quad+(m_2l_2^2+m_2l_1l_2\cos\phi_2)\ddot{\phi}_2-m_2l_1l_2\sin\phi_2\dot{\phi}_2^2\\&\quad-2m_2l_1l_2\sin\phi_2\dot{\phi}_1\dot{\phi}_2+(m_1+m_2)gl_1\sin\phi_1\\&\quad+m_2gl_2\sin(\phi_1+\phi_2)=0,\end{aligned}\tag{26}$$

$$\begin{aligned}&(m_2l_1l_2\cos\phi_2+m_2l_2^2)\ddot{\phi}_1+m_2l_2^2\ddot{\phi}_2+m_2l_1l_2\sin\phi_2\dot{\phi}_1^2\\&\quad+m_2gl_2\sin(\phi_1+\phi_2)+k\phi_2=0.\end{aligned}\tag{27}$$

Dividing both sides of (25) with m_2l_2 gives that

$$\begin{aligned}&\beta\left(\ddot{\phi}_1\cos\phi_1-\dot{\phi}_1^2\sin\phi_1\right)+\left[(\ddot{\phi}_1+\ddot{\phi}_2)\cos(\phi_1+\phi_2)\right.\\&\qquad\left.-(\dot{\phi}_1+\dot{\phi}_2)^2\sin(\phi_1+\phi_2)\right]=c_2,\end{aligned}\tag{28}$$

where β and c_2 are constants with the following expressions:

$$\begin{aligned}\beta&=\frac{(m_1+m_2)l_1}{m_2l_2},\\c_2&=-\frac{c_1\left(k_p+k_\chi\left[\frac{x_d-x_M}{(\lambda-x_M)^3}+\frac{x_d-x_m}{(\lambda-x_m)^3}\right]\right)}{m_2l_2}.\end{aligned}\tag{29}$$

Then, integrating both sides of (28) with time t shows that

$$\beta\dot{\phi}_1\cos\phi_1+(\dot{\phi}_1+\dot{\phi}_2)\cos(\phi_1+\phi_2)=c_2t+c_3,\tag{30}$$

where c_3 denotes a constant. It has been proved in (20) that $\dot{\phi}_1$ and $\dot{\phi}_2$ are bounded signals; then, accordingly, the left side of (30) is bounded. If c_2 is nonzero, then when $t\to\infty$, one has $c_2t+c_3\to\infty$, which contradicts the conclusion that the left side in (30) is bounded. Therefore, the value of c_2 should be zero. In the meantime, by using the conclusion in (19) and $x_M\geq x_d$, $x_m<x_d$, one has

$$k_p+k_\chi\left[\frac{x_d-x_M}{(\lambda-x_M)^3}+\frac{x_d-x_m}{(\lambda-x_m)^3}\right]>0,\tag{31}$$

Since it has been proved that c_2 must be 0, the conclusion of $c_1=0$ can be obtained by using (29) and (31). Further, in accordance with (24), it is easy to know that $e=0$. Then, within S, the following result holds:

$$x=x_d.\tag{32}$$

Together with $c_2=0$, (30) can be organized as

$$\beta\dot{\phi}_1\cos\phi_1+(\dot{\phi}_1+\dot{\phi}_2)\cos(\phi_1+\phi_2)=c_3.\tag{33}$$

By integrating (33), one has

$$\beta\sin\phi_1+\sin(\phi_1+\phi_2)=c_3t+c_4,\tag{34}$$

where c_4 represents a constant. Taking account of the fact that $\sin\phi_1$ and $\sin(\phi_1+\phi_2)$ are bounded, it is not difficult to know that c_3 should be zero after a similar analysis. Hence, (33) can be rewritten as

$$\beta\dot{\phi}_1\cos\phi_1+(\dot{\phi}_1+\dot{\phi}_2)\cos(\phi_1+\phi_2)=0.\tag{35}$$

Furthermore, by inserting $c_3=0$ into (34), we can obtain

$$\beta\sin\phi_1+\sin(\phi_1+\phi_2)=c_4.\tag{36}$$

Then, by dividing (26) with regard to $m_2l_1l_2$, and together with (36), the following results can be produced:

$$\begin{aligned}&\left(\beta+\frac{l_2}{l_1}\right)\ddot{\phi}_1+\frac{l_2}{l_1}\ddot{\phi}_2+2\cos\phi_2\ddot{\phi}_1-2\sin\phi_2\dot{\phi}_1\dot{\phi}_2\\&\quad+\cos\phi_2\ddot{\phi}_2-\sin\phi_2\dot{\phi}_2^2=-\frac{\beta\sin\phi_1+\sin(\phi_1+\phi_2)}{l_1}g\\&\qquad=-\frac{c_4}{l_1}g,\end{aligned}\tag{37}$$

which further implies that

$$\begin{aligned}&\left(\beta+\frac{l_2}{l_1}\right)\dot{\phi}_1+\frac{l_2}{l_1}\dot{\phi}_2+2\cos\phi_2\dot{\phi}_1+\cos\phi_2\dot{\phi}_2\\&\qquad=-\frac{c_4}{l_1}gt+c_5,\end{aligned}\tag{38}$$

where c_5 denotes a constant. Since both $\dot{\phi}_1$ and $\dot{\phi}_2$ are proved to be bounded signals, on the basis of the boundedness analysis of the signals in (38), one concludes that $c_4=0$. Furthermore, according to (36), it can be seen that

$$\beta\sin\phi_1+\sin(\phi_1+\phi_2)=0.\tag{39}$$

Equation (38) can be further simplified to

$$\left(\beta+\tfrac{l_2}{l_1}\right)\dot{\phi}_1+\tfrac{l_2}{l_1}\dot{\phi}_2+\cos\phi_2(2\dot{\phi}_1+\dot{\phi}_2)=c_5.\tag{40}$$

On the other hand, one has

$$\begin{aligned}\cos\phi_2&=\cos[(\phi_1+\phi_2)-\phi_1]\\&=\cos(\phi_1+\phi_2)\cos\phi_1+\sin(\phi_1+\phi_2)\sin\phi_1,\end{aligned}\tag{41}$$

Thus, one has that

$$\begin{aligned}&\cos\phi_2(2\dot{\phi}_1+\dot{\phi}_2)\\&=\cos\phi_2[\dot{\phi}_1+(\dot{\phi}_1+\dot{\phi}_2)]\\&=\dot{\phi}_1\cos(\phi_1+\phi_2)\cos\phi_1+(\dot{\phi}_1+\dot{\phi}_2)\sin(\phi_1+\phi_2)\sin\phi_1\\&\quad+(\dot{\phi}_1+\dot{\phi}_2)\cos(\phi_1+\phi_2)\cos\phi_1+\dot{\phi}_1\sin(\phi_1+\phi_2)\sin\phi_1.\end{aligned}\tag{42}$$

From (35) and (39), we can further rearrange (42) as follows:

$$\begin{aligned}&\cos\phi_2(2\dot{\phi}_1+\dot{\phi}_2)\\&=-\frac{1}{\beta}(\dot{\phi}_1+\dot{\phi}_2)[\sin^2(\phi_1+\phi_2)+\cos^2(\phi_1+\phi_2)]\\&\quad-\beta\dot{\phi}_1(\sin^2\phi_1+\cos^2\phi_1)\\&=-\frac{1}{\beta}(\dot{\phi}_1+\dot{\phi}_2)-\beta\dot{\phi}_1.\end{aligned}\tag{43}$$

Then, by substituting (43) into (40), we can obtain that

$$\left(\frac{l_2}{l_1}-\frac{1}{\beta}\right)(\dot{\phi}_1+\dot{\phi}_2)=c_5,\tag{44}$$

that is,

$$\dot{\phi}_1 + \dot{\phi}_2 = \frac{c_5}{\left(\frac{l_2}{l_1} - \frac{1}{\beta}\right)} = c_6, \tag{45}$$

wherein c_6 is a constant. In addition, integrating both sides of (45) with time yields

$$\phi_1 + \phi_2 = c_6 t + c_7, \tag{46}$$

with c_7 denotes a constant. As per Assumption 1, one can obtain $c_6 = 0$. Then, it is further easy to obtain by (45) that

$$\dot{\phi}_1 + \dot{\phi}_2 = 0; \tag{47}$$

then, we substitute (47) into (35) to drive that

$$\beta \dot{\phi}_1 \cos\phi_1 = 0. \tag{48}$$

From Assumption 1, one has $\cos\phi_1 \neq 0$, and thus,

$$\dot{\phi}_1 = 0. \tag{49}$$

By further substituting (49) into (47), one has

$$\dot{\phi}_2 = 0. \tag{50}$$

Hence, it can directly lead to the following result:

$$\ddot{\phi}_1 = 0, \ \ddot{\phi}_2 = 0. \tag{51}$$

Substituting (49), (50), and (51) into (27) yields that

$$\begin{aligned} &m_2 g l_2 \sin(\phi_1 + \phi_2) + k\phi_2 = 0 \\ &\Rightarrow \frac{k}{m_2 g l_2}\phi_2 = -\sin(\phi_1 + \phi_2). \end{aligned} \tag{52}$$

In addition, it is further implied from (39) that

$$\beta \sin\phi_1 = -\sin(\phi_1 + \phi_2), \tag{53}$$

Then, using (52) with (53), we can obtain that

$$\beta \sin\phi_1 = \frac{k}{m_2 g l_2}\phi_2. \tag{54}$$

At the same time, from Assumption 1, it is not difficult to know that the signs of ϕ_1 and $\sin\phi_1$ are the same. Furthermore, according to (54), we can see that ϕ_1 and ϕ_2 also have the same sign.

Next, we will prove that the conclusion of $\phi_1 = 0, \ \phi_2 = 0$ in the invariant set S is valid. For this purpose, the following three cases are considered:

Case 1 ($0 < \phi_1 < \frac{\pi}{2}$)*:* Since ϕ_2 and ϕ_1 have the same sign, from Assumption 1, it can be known that if $0 < \phi_2 < \frac{\pi}{2}$, then $0 < \phi_1 + \phi_2 < \pi$. Therefore, we can further draw the following conclusion:

$$\begin{aligned} &\sin\phi_1 > 0, \sin(\phi_1 + \phi_2) > 0 \\ &\Rightarrow \beta \sin\phi_1 + \sin(\phi_1 + \phi_2) > 0, \end{aligned} \tag{55}$$

which is inconsistent with the proved result in (39). As a consequence, Case 1 is not valid.

Case 2 ($-\frac{\pi}{2} < \phi_1 < 0$)*:* According to some analysis similar to Case 1, if $-\frac{\pi}{2} < \phi_2 < 0$, then one has $-\pi < \phi_1 + \phi_2 < 0$, and

$$\begin{aligned} &\sin\phi_1 < 0, \sin(\phi_1 + \phi_2) < 0 \\ &\Rightarrow \beta \sin\phi_1 + \sin(\phi_1 + \phi_2) < 0, \end{aligned} \tag{56}$$

which again contradicts (39).

Case 3 ($\phi_1 = 0$)*:* By inserting $\phi_1 = 0$ into (54), we can derive that $\phi_2 = 0$. Then, $\beta \sin\phi_1 + \sin(\phi_1 + \phi_2) = 0$ is valid at this time, which satisfies the conclusion in (39).

In summary, only Case 3 holds, that is, $\phi_1 = 0, \ \phi_2 = 0$ holds in the invariant set S. As a summary, in S, one has

$$x = x_d, \ \dot{x} = 0, \ \phi_1 = 0, \ \dot{\phi}_1 = 0, \ \phi_2 = 0, \ \dot{\phi}_2 = 0. \tag{57}$$

Furthermore, in accordance with LaSalle's invariance principle, the results of Theorem 1 hold. □

Remark 1: The derived model in (4)-(6) for flexible rope cranes is different from that for double-pendulum cranes, e.g., in [26]. One difference lies in that a virtual spring which reflect the flexible vibration is added, which makes the controller design and analysis much different. On the other hand, the designed controller (16) and corresponding stability analysis are also different from those of existing control methods for double-pendulum cranes, e.g., [26].

IV. EXPERIMENTS AND ANALYSIS

As a means to test the effectiveness of the presented control approach, we test its control performance on the self-built hardware experimental platform in Fig. 2.

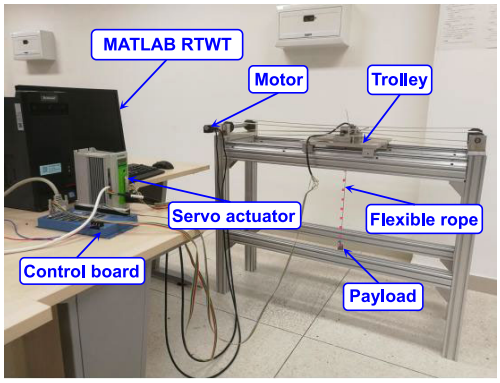

FIGURE 2. The self-built flexible rope crane experimental platform.

The hardware platform is composed of the mechanical body, the driving devices, the measuring devices, and the control system. The mechanical body, which includes the mechanical structure, the trolley, the payload, and the flexible rope, is the skeleton of the entire experimental platform. It is worth noting that we choose a flexible rope, which is prone to bend, as the crane rope for the purpose of reflecting the characteristics of flexible rope cranes. An AC servo motor (100W) is selected as the driving device to control the trolley. Moreover, measuring devices are primarily responsible for measuring the trolley displacement and the

payload swing angle. The displacement can be obtained by the encoder equipped inside the AC servo motor. For swing angle measurement, it is necessary to point out that the swing angle defined in this paper is different from that of rigid rope cranes, and it cannot be directly obtained by encoders. Hence, we introduce the method of computer vision and machine learning algorithms to obtain the payload swing angle. Moreover, the rope's horizontal deformation is measured in the same way. Finally, the control system consists of a PC equipped with MATLAB/Simulink Real Time Windows Target (RTWT), which is used to achieve real-time control of the hardware platform, and the sampling time is 5 ms. In addition, the control system also includes a motion control board, which can collect data from encoders, convert the control commands sent by the PC to the corresponding control signals, and then deliver them to the driving devices.

Furthermore, the parameters of the experimental platform are as follows:

$$M = 6.5 \text{ kg}, \ l = 0.6 \text{ m}.$$

Without losing generality, in each group of experiments, the initial and target position of the trolley are set as $x(0) = 0.05$ m, $x_d = 0.6$ m. At the same time, the lower and upper bounds of the trolley motion range are selected as $x_m = 0.01$ m, $x_M = 0.8$ m. The control gains in the controller (16) and the parameters in the velocity estimator (11) are chosen easily as follows:

$$k_p = 26, \ k_v = 3, \ k_\chi = 0.01, \ m_v = 1, \ c = 1.$$

In this paper, three groups of experimental results are exhibited to demonstrate the effectiveness and robustness of the designed controller. For the first group of experiments, the payload mass is set as 0.3 kg. To verify the anti-disturbance ability of the control method, in the second group of experiments, we will impose initial disturbance and external disturbance on the payload, respectively. Furthermore, in the third group of experiments, the payload mass is adjusted from 0.3 kg to 0.8 kg to test the robustness of the proposed method in the face of system parameters uncertainty.

A. EXPERIMENT 1

The results of the first group of experiments are shown in Figs. 3-4. The curves from the top to the bottom in Fig. 3 show the trolley displacement, the payload swing angle, and the control force input, respectively. From the trolley displacement curve, it can be seen that the trolley arrives at the given position quickly and accurately in about 3 seconds. At the same time, during the entire process, the trolley is always within the given range. Moreover, there is almost no residual payload swing, after the trolley arrives at the target position. In Fig. 4, the three-dimensional plot of the crane rope is given, which describes the variation of each point on the crane rope with time. It can be seen that, under the action of the proposed controller, the flexible characteristics of the crane rope are effectively suppressed, and its maximum bending deformation is limited to less than 0.04 m.

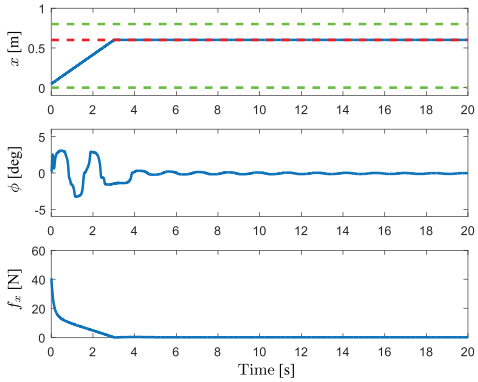

FIGURE 3. Experiment 1: the proposed method (solid line: experiment results, red dashed line: target trolley position, green dashed line: upper and lower bounds of the trolley motion range).

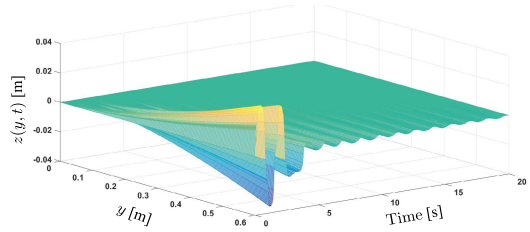

FIGURE 4. Experiment 1: position $z(y, t)$ of the flexible rope.

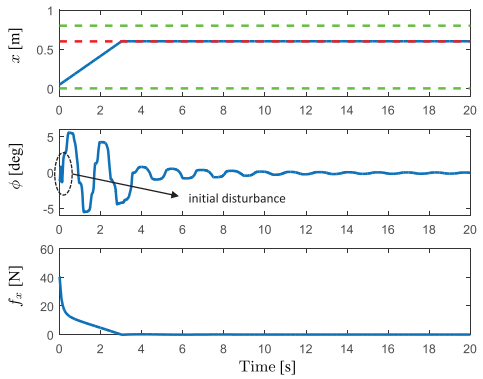

FIGURE 5. Experiment 2 – Case 1: the proposed method (solid line: experiment results, red dashed line: target trolley position, green dashed line: upper and lower bounds of the trolley motion range).

B. EXPERIMENT 2

The results of Experiment 2 are shown in Figs. 5-8. As can be seen from Fig. 5, when the initial payload swing angle is not zero (approximately 1.5 deg) due to the initial disturbance, the designed controller can still achieve satisfactory performance. The trolley can achieve precise positioning in a relatively short time, and does not exceed the given range from the beginning to the end. In addition, the payload swing angle converges to zero quickly. The experimental results in Fig. 7 show that the added disturbance effects are quickly

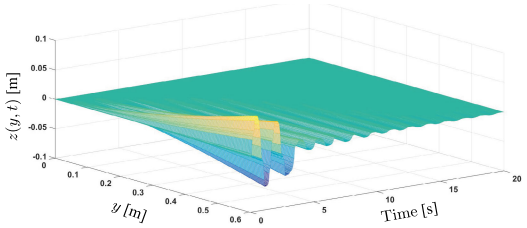

FIGURE 6. Experiment 2 – Case 1: position $z(y, t)$ of the flexible rope.

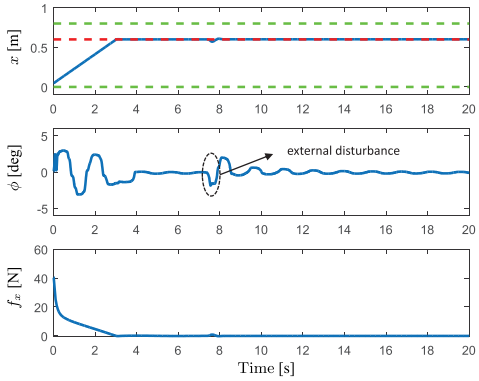

FIGURE 7. Experiment 2 – Case 2: the proposed method (solid line: experiment results, red dashed line: target trolley position, green dashed line: upper and lower bounds of the trolley motion range).

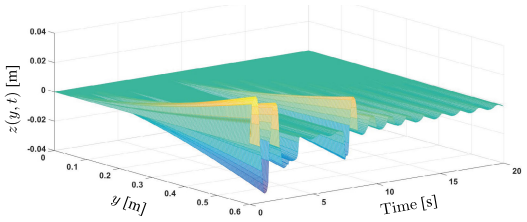

FIGURE 8. Experiment 2 – Case 2: position $z(y, t)$ of the flexible rope.

eliminated, and the payload returns to the steady state within about two periods. Furthermore, the three-dimensional plots in Fig. 6 and Fig. 8 show that the bending deformation of the crane rope can be limited to a reasonable range even in the presence of external disturbances. In conclusion, the experimental results show that the proposed method shows good anti-disturbance ability and can maintain satisfactory control performance under disturbances.

C. EXPERIMENT 3

In the third group of experiments, the payload mass is adjusted from 0.3 kg to 0.8 kg, while the control parameters are unchanged, so as to test the adaptive ability of the proposed control scheme in parametrical uncertainties. The experimental results are shown in Figs. 9-10. It can be seen that the tasks of trolley positioning, payload swing suppression, and flexible rope bending restraining, are effectively achieved, despite the change of the payload mass.

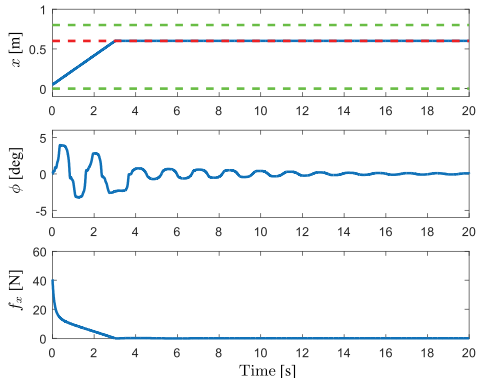

FIGURE 9. Experiment 3: the proposed method (solid line: experiment results, red dashed line: the target position of trolley, green dashed line: the upper and lower bounds of the trolley motion range).

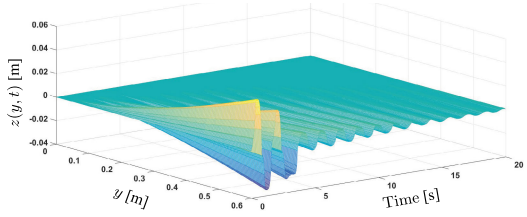

FIGURE 10. Experiment 3: position $z(y, t)$ of the flexible rope.

V. CONCLUSION

In many application scenarios, the crane rope will inevitably bend, which will aggravate the payload swing and seriously affect the efficiency and safety of crane systems. Therefore, it is of great theoretical and practical significance to analyze the rope's flexible characteristics and achieve effective control results. To do so, this paper has designed a nonlinear output feedback control scheme for flexible rope crane systems. In particular, by analyzing the system energy, a nonlinear controller is proposed, which does not need velocity signals for feedback and can restrict the trolley motion always within a safe range. Detailed mathematical analysis is provided to prove the closed-loop stability. Finally, a series of hardware experimental results verify the satisfactory performance of the designed controller in terms of effectiveness and robustness.

ACKNOWLEDGMENT

The authors are very grateful to all the reviewers and the handling Associate Editor for the helpful comments, which are very important for improving the quality of the presentation. *(Ning Sun and Jianyi Zhang contributed equally to this paper).*

REFERENCES

[1] W. Sun, S.-F. Su, J. Xia, and V.-T. Nguyen, "Adaptive fuzzy tracking control of flexible-joint robots with full-state constraints," *IEEE Trans. Syst., Man, Cybern. Syst.*, to be published. doi: 10.1109/TSMC.2018.2870642.
[2] X. Xin, "Analysis of the energy-based swing-up control for the double pendulum on a cart," *Int. J. Robust Nonlinear Control*, vol. 21, no. 4, pp. 387–403, Mar. 2011.

[3] Z. Zhao, C. K. Ahn, and H.-X. Li, "Boundary anti-disturbance control of a spatially nonlinear flexible string system," *IEEE Trans. Ind. Electron.*, to be published. doi: 10.1109/TIE.2019.2931230.

[4] Y. Wu, N. Sun, Y. Fang, and D. Liang, "An increased nonlinear coupling motion controller for underactuated multi-TORA systems: Theoretical design and hardware experimentation," *IEEE Trans. System, Man, Cybern. Syst.*, vol. 49, no. 6, pp. 1186–1193, Jun. 2019.

[5] X. Xin and Y. Liu, "A set-point control for a two-link underactuated robot with a flexible elbow joint," *ASME J. Dyn. Syst., Meas., Control*, vol. 135, no. 5, Sep. 2013, Art. no. 051016.

[6] S. Li, J. Li, and Y. Mo, "Piezoelectric multimode vibration control for stiffened plate using ADRC-based acceleration compensation," *IEEE Trans. Ind. Electron.*, vol. 61, no. 12, pp. 6892–6902, Dec. 2014.

[7] S. Hou, J. Fei, C. Chen, and Y. Chu, "Finite-time adaptive fuzzy-neural-network control of active power filter," *IEEE Trans. Power Electron.*, vol. 34, no. 10, pp. 10298–10313, Oct. 2019.

[8] N. Sun, D. Liang, Y. Wu, Y. Chen, Y. Qin, and Y. Fang, "Adaptive control for pneumatic artificial muscle systems with parametric uncertainties and unidirectional input constraints," *IEEE Trans. Ind. Informat.*, to be published. doi: 10.1109/TII.2019.2923715.

[9] Q. Zhou, S. Zhao, H. Li, R. Lu, and C. Wu, "Adaptive neural network tracking control for robotic manipulators with dead zone," *IEEE Trans. Neural Netw. Learn. Syst.*, to be published. doi: 10.1109/TNNLS.2018.2869375.

[10] H. Li, W. Yan, and Y. Shi, "Continuous-time model predictive control of under-actuated spacecraft with bounded control torques," *Automatica*, vol. 75, pp. 144–153, Jan. 2017.

[11] Y. Sun, J. Xu, H. Qiang, and G. Lin, "Adaptive neural-fuzzy robust position control scheme for maglev train systems with experimental verification," *IEEE Trans. Ind. Electron.*, vol. 66, no. 11, pp. 8589–8599, Nov. 2019.

[12] H. Li, S. Zhao, W. He, and R. Lu, "Adaptive finite-time tracking control of full state constrained nonlinear systems with dead-zone," *Automatica*, vol. 100, pp. 99–107, Feb. 2019.

[13] M. N. Abourraja, M. Oudani, M. Y. Samiri, D. Boudebous, A. E. Fazziki, M. Najib, A. Bouain, and N. Rouky, "A multi-agent based simulation model for rail–rail transshipment: An engineering approach for gantry crane scheduling," *IEEE Access*, vol. 5, pp. 13142–13156, 2017.

[14] S. Yang and B. Xian, "Energy-based nonlinear adaptive control design for the quadrotor UAV system with a suspended payload," *IEEE Trans. Ind. Electron.*, to be published. doi: 10.1109/TIE.2019.2902834.

[15] G. Tang, C. Shi, Y. Wang, and X. Hu, "Strength analysis of the main structural component in ship-to-shore cranes under dynamic load," *IEEE Access*, vol. 7, pp. 23959–23966, 2019.

[16] M. J. Maghsoudi, Z. Mohamed, S. Sudin, S. Buyamin, H. I. Jaafar, and S. M. Ahmadc, "An improved input shaping design for an efficient sway control of a nonlinear 3D overhead crane with friction," *Mech. Syst. Signal Process.*, vol. 92, pp. 364–378, Aug. 2017.

[17] W. Singhose, D. Kim, and M. Kenison, "Input shaping control of double-pendulum bridge crane oscillations," *ASME J. Dyn. Syst., Meas., Control*, vol. 130, no. 3, May 2008, Art. no. 034504.

[18] J. Huang, X. Xie, and Z. Liang, "Control of bridge cranes with distributed-mass payload dynamics," *IEEE/ASME Trans. Mechatronics*, vol. 20, no. 1, pp. 481–486, Feb. 2015.

[19] K. T. Hong, C. D. Huh, and K.-S. Hong, "Command shaping control for limiting the transient sway angle of crane systems," *Int. J. Control Autom. Syst.*, vol. 1, no. 1, pp. 43–53, Mar. 2003.

[20] H.-H. Lee, "Motion planning for three-dimensional overhead cranes with high-speed load hoisting," *Int. J. Control*, vol. 78, no. 12, pp. 875–886, Aug. 2005.

[21] N. Uchiyama, H. Ouyang, and S. Sano, "Simple rotary crane dynamics modeling and open-loop control for residual load sway suppression by only horizontal boom motion," *Mechatronics*, vol. 23, no. 8, pp. 1223–1236, Dec. 2013.

[22] N. Sun, Y. Wu, H. Chen, and Y. Fang, "An energy-optimal solution for transportation control of cranes with double pendulum dynamics: Design and experiments," *Mech. Syst. Signal Process.*, vol. 102, pp. 87–101, Mar. 2018.

[23] S. Küchler, T. Mahl, J. Neupert, K. Schneider, and O. Sawodny, "Active control for an offshore crane using prediction of the vessel's motion," *IEEE/ASME Trans. Mechatronics*, vol. 16, no. 2, pp. 297–309, Apr. 2011.

[24] Z. Zhang, Y. Wu, and J. Huang, "Differential-flatness-based finite-time anti-swing control of underactuated crane systems," *Nonlinear Dyn.*, vol. 87, no. 3, pp. 1749–1761, Feb. 2017.

[25] M. Zhang, X. Ma, X. Rong, X. Tian, and Y. Li, "Error tracking control for underactuated overhead cranes against arbitrary initial payload swing angles," *Mech. Syst. Signal Process.*, vol. 84, pp. 268–285, Feb. 2017.

[26] N. Sun, Y. Fang, H. Chen, and B. Lu, "Amplitude-saturated nonlinear output feedback antiswing control for underactuated cranes with double-pendulum cargo dynamics," *IEEE Trans. Ind. Electron.*, vol. 64, no. 3, pp. 2135–2146, Mar. 2017.

[27] X. Wu and X. He, "Enhanced damping-based anti-swing control method for underactuated overhead cranes," *IET Control Theory Appl.*, vol. 9, no. 12, pp. 1893–1900, Aug. 2015.

[28] N. Sun, T. Yang, Y. Fang, B. Lu, and Y. Qian, "Nonlinear motion control of underactuated three-dimensional boom cranes with hardware experiments," *IEEE Trans. Ind. Informat.*, vol. 14, no. 3, pp. 887–897, Mar. 2018.

[29] N. Sun, Y. Fang, H. Chen, Y. Fu, and B. Lu, "Nonlinear stabilizing control for ship-mounted cranes with ship roll and heave movements: Design, analysis, and experiments," *IEEE Trans. Syst., Man, Cybern. Syst.*, vol. 48, no. 10, pp. 1781–1793, Oct. 2018.

[30] H. Ouyang, J. Wang, G. Zhang, L. Mei, and X. Deng, "Novel adaptive hierarchical sliding mode control for trajectory tracking and load sway rejection in double-pendulum overhead cranes," *IEEE Access*, vol. 7, pp. 10353–10361, 2019.

[31] A. T. Le and S.-G. Lee, "3D cooperative control of tower cranes using robust adaptive techniques," *J. Franklin Inst.*, vol. 354, no. 18, pp. 8333–8357, Dec. 2017.

[32] J. Yang and K. Yang, "Adaptive coupling control for overhead crane systems," *Mechatronics*, vol. 17, nos. 2–3, pp. 143–152, Mar./Apr. 2007.

[33] N. Sun, T. Yang, H. Chen, Y. Fang, and Y. Qian, "Adaptive anti-swing and positioning control for 4-DOF rotary cranes subject to uncertain/unknown parameters with hardware experiments," *IEEE Trans. Syst., Man, Cybern. Syst.*, vol. 49, no. 7, pp. 1309–1321, Jul. 2019.

[34] N. Sun, Y. Wu, H. Chen, and Y. Fang, "Antiswing cargo transportation of underactuated tower crane systems by a nonlinear controller embedded with an integral term," *IEEE Trans. Autom. Sci. Eng.*, vol. 16, no. 3, pp. 1387–1398, Jul. 2019.

[35] Q. H. Ngo and K.-S. Hong, "Sliding-mode antisway control of an offshore container crane," *IEEE/ASME Trans. Mechtronics*, vol. 17, no. 2, pp. 201–209, Apr. 2012.

[36] M. S. Park, D. Chwa, and M. Eom, "Adaptive sliding-mode antisway control of uncertain overhead cranes with high-speed hoisting motion," *IEEE Trans. Fuzzy Syst.*, vol. 22, no. 5, pp. 1262–1271, Oct. 2014.

[37] C. Vázquez, J. Collado, and L. Fridman, "Control of a parametrically excited crane: A vector Lyapunov approach," *IEEE Trans. Control Syst. Technol.*, vol. 21, no. 6, pp. 2332–2340, Nov. 2013.

[38] Q. H. Ngo and K.-S. Hong, "Adaptive sliding mode control of container cranes," *IET Control Theory Appl.*, vol. 6, no. 5, pp. 662–668, Mar. 2012.

[39] O. Sawodny, H. Aschemann, and S. Lahres, "An automated gantry crane as a large workspace robot," *Control Eng. Pract.*, vol. 10, no. 12, pp. 1323–1338, Dec. 2002.

[40] N. Sun, T. Yang, Y. Fang, Y. Wu, and H. Chen, "Transportation control of double-pendulum cranes with a nonlinear quasi-PID scheme: Design and experiments," *IEEE Trans. Syst., Man, Cybern. Syst.*, vol. 49, no. 7, pp. 1408–1418, Jul. 2019.

[41] A. Piazzi and A. Visioli, "Optimal dynamic-inversion-based control of an overhead crane," *IEE Proc.-Control Theory Appl.*, vol. 149, no. 5, pp. 405–411, Sep. 2002.

[42] G. Boschetti, R. Caracciolo, D. Richiedei, and A. Trevisani, "A non-time based controller for load swing damping and path-tracking in robotic cranes," *J. Intell. Robot. Syst.*, vol. 76, no. 2, pp. 201–217, Nov. 2014.

[43] Y. Zhao and H. Gao, "Fuzzy-model-based control of an overhead crane with input delay and actuator saturation," *IEEE Trans. Fuzzy Syst.*, vol. 20, no. 1, pp. 181–186, Feb. 2012.

[44] Q. H. Ngo, N. P. Nguyen, C. N. Nguyen, T. H. Tran, and K.-S. Hong, "Fuzzy sliding mode control of container cranes," *Int. J. Control, Autom. Syst.*, vol. 13, no. 2, pp. 419–425, Apr. 2015.

[45] J. Smoczek and J. Szpytko, "Particle swarm optimization-based multivariable generalized predictive control for an overhead crane," *IEEE/ASME Trans. Mechtronics*, vol. 22, no. 1, pp. 258–268, Jun. 2017.

[46] Z. Sun, Y. Bi, X. Zhao, Z. Sun, C. Ying, and S. Tan, "Type-2 fuzzy sliding mode anti-swing controller design and optimization for overhead crane," *IEEE Access*, vol. 6, pp. 51931–51938, 2018.

[47] C. Y. Chang, "Adaptive fuzzy controller of the overhead cranes with nonlinear disturbance," *IEEE Trans Ind. Informat.*, vol. 3, no. 2, pp. 164–172, May 2007.

[48] D. Qian, S. Tong, and S. Lee, "Fuzzy-logic-based control of payloads subjected to double-pendulum motion in overhead cranes," *Automat. Construct.*, vol. 65, pp. 133–143, May 2016.
[49] R. Toxqui, W. Yu, and X. Li, "Anti-swing control for overhead crane with neural compensation," in *Proc. Int. Joint Conf. Neural Netw.*, Vancouver, BC, Canada, Jul. 2006, pp. 4697–4703.
[50] T. Yang, N. Sun, H. Chen, and Y. Fang, "Neural network-based adaptive antiswing control of an underactuated ship-mounted crane with roll motions and input dead zones," *IEEE Trans. Neural Netw. Learn. Syst.*, to be published. doi: 10.1109/TNNLS.2019.2910580.
[51] M. I. Solihin, Wahyudi, and A. Albagul, "Development of soft sensor for sensorless automatic gantry crane using RBF neural networks," in *Proc. IEEE Conf. Cybern. Intell. Syst.*, Bangkok, Thailand, Jun. 2006, pp. 1–6.
[52] U. H. Shah and K.-S. Hong, "Active vibration control of a flexible rod moving in water: Application to nuclear refueling machines," *Automatica*, vol. 93, pp. 231–243, Jul. 2018.
[53] W. He, S. Zhang, and S. S. Ge, "Adaptive control of a flexible crane system with the boundary output constraint," *IEEE Trans. Ind. Electron.*, vol. 61, no. 8, pp. 4126–4133, Aug. 2014.
[54] W. He and S. S. Ge, "Cooperative control of a nonuniform gantry crane with constrained tension," *Automatica*, vol. 66, pp. 146–154, Apr. 2016.
[55] B. D'Andréa-Novel, F. Boustany, F. Conrad, and B. P. Rao, "Feedback stabilization of a hybrid PDE-ODE system: Application to an overhead crane," *Math. Control, Signals Syst.*, vol. 7, no. 1, pp. 1–22, Mar. 1994.
[56] B. D' Andréa-Novel and J. M. Coron, "Exponential stabilization of an overhead crane with flexible cable via a back-stepping approach," *Automatica*, vol. 36, no. 4, pp. 587–593, Apr. 2000.

NING SUN (S'12–M'14–SM'19) received the B.S. degree (Hons.) in measurement and control technology and instruments from Wuhan University, Wuhan, China, in 2009, and the Ph.D. degree (Hons.) in control theory and control engineering from Nankai University, Tianjin, China, in 2014, where he is currently an Associate Professor with the Institute of Robotics and Automatic Information Systems.

He is also a JSPS International Research Fellow with the Faculty of Computer Science and Systems Engineering, Okayama Prefectural University, from November 2018 to October 2019. His research interests include underactuated systems (e.g., cranes) and nonlinear control with applications to mechatronic systems.

Dr. Sun received the First Class Prize of the Wu Wen Jun Artificial Intelligence Natural Science Award, the First Class Prize of the Tianjin Natural Science Award, the Golden Patent Award of Tianjin, the International Journal of Control, Automation, and Systems (IJCAS) Academic Activity Award, and the Outstanding Ph.D. Dissertation Award from the Chinese Association of Automation (CAA), and so on. He is the Executive Editor for *Measurement and Control* and serves as an Associate Editor (editorial board member) for several journals, including IEEE Access, *International Journal of Control, Automation, and Systems*, *Transactions of the Institute of Measurement and Control*, *International Journal of Precision Engineering and Manufacturing*, and so on. He has been an Associate Editor of the IEEE Control Systems Society (CSS) Conference Editorial Board, since July 2019.

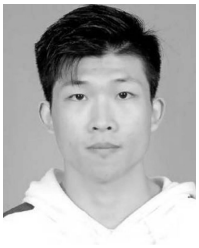

JIANYI ZHANG received the B.S. degree in electrical engineering and automation from Shandong Jianzhu University, Jinan, China, in 2017. He is currently pursuing the M.S. degree in control science and engineering with the Institute of Robotics and Automatic Information Systems, Nankai University, Tianjin, China, under the supervision of Dr. Ning Sun.

His research interests include the dynamic modeling and control of flexible cable cranes.

XIN XIN (S'94–A'95–M'02–SM'08) received the B.S. degree from the University of Science and Technology of China, Hefei, China, in 1987, the Ph.D. degree from Southeast University, Nanjing, China, in 1993, and the Ph.D. degree in engineering from the Tokyo Institute of Technology, in 2000.

From 1991 to 1993, he did his Ph.D. studies in Osaka University as a co-advised student of China and Japan with the Japanese Government Scholarship. From 1993 to 1995, he was a Postdoctoral Researcher and then became an Associate Professor with Southeast University. From 1996 to 1997, he was with the New Energy and Industrial Technology Development, Japan, as an Advanced Industrial Technology Researcher. From 1997 to 2000, he was a Research Associate of the Tokyo Institute of Technology. Since 2000, he has been with Okayama Prefectural University as an Associate Professor, where he has been a Professor, since 2008. His current research interests include robotics, dynamics, and control of nonlinear underactuated systems.

He received the Division Paper Award of SICE 3rd Annual Conference on Control Systems, in 2004. He is an Associate Editor of the IEEE Control Systems Letters (L-CSS).

TONG YANG received the B.S. degree in automation from Nankai University, Tianjin, China, in 2017, where she is currently pursuing the Ph.D. degree in control science and engineering with the Institute of Robotics and Automatic Information Systems, under the supervision of Dr. Ning Sun.

Her research interests include the nonlinear control of underactuated systems, including rotary cranes, offshore cranes, and tower cranes.

YONGCHUN FANG (S'00–M'02–SM'08) received the B.S. and M.S. degrees in control theory and applications from Zhejiang University, Hangzhou, China, in 1996 and 1999, respectively, and the Ph.D. degree in electrical engineering from Clemson University, Clemson, SC, in 2002.

From 2002 to 2003, he was a Postdoctoral Fellow with the Sibley School of Mechanical and Aerospace Engineering, Cornell University, Ithaca, NY. He is currently a Professor with the Institute of Robotics and Automatic Information Systems, Nankai University, Tianjin, China. His research interests include nonlinear control, visual servoing, control of underactuated systems, and AFM-based nanosystems. He was an Associate Editor of ASME *Journal of Dynamic Systems, Measurement and Control*.